Taylor's power law captures the effects of environmental variability on community structure: An example from fishes in the North Sea

Keywords:

mean-variance scaling; aggregation; spatial patchiness; temporal fluctuations; ecosystem metrics; fish community

Authors:

Matthew R. D. Cobain[1] – matthew.cobain@newcastle.ac.uk, Markus Brede[2] – Markus.Brede@soton.ac.uk, and Clive N. Trueman[1] – trueman@noc.soton.ac.uk

1. Ocean and Earth Science, University of Southampton, Waterfront Campus, NOCS, Southampton, UK
2. Agents, Interaction and Complexity Group, Electronics and Computer Science, University of Southampton, Highfield Campus, Southampton, UK

Statement of Authorship:

MRDC processed data, conducted statistical analyses and wrote first manuscript draft, CNT conceptualised the study and all authors contributed equally to study development and manuscript review and editing.

Data accessibility statement:

All data used in this study are publicly available online. NS-IBTS data was accessed via the DATRAS data portal (http://www.ices.dk/marine-data/data-portals/Pages/DATRAS.aspx - accessed 03/09/2015). The ETOPO1 1arc-minute global relief model was accessed via the NOAA metadata bank (Doi:10.7289/V5C8276M).

Abstract

1. Taylor's power law (TPL) describes the relationship between the mean and variance in abundance of populations, with the power law exponent considered a measure of aggregation. However the usefulness of TPL exponents as an ecological metric has been questioned, largely due to its apparent ubiquity in various complex systems.

2. The aim of this study was to test whether TPL exponents vary systematically with potential drivers of animal aggregation in time and space, and therefore capture useful ecological information of the system of interest.

3. We derived community TPL exponents from a long term, standardised and spatially dense data series of abundance and body size data for a strongly size-structured fish community in the North Sea. We then compared TPL exponents between regions of contrasting environmental characteristics.

4. We find that, in general, TPL exponents vary more than expected under random conditions in the North Sea for size-based populations compared to communities considered by species. Further, size-based temporal TPL exponents are systematically higher (implying more temporally-aggregated distributions) along hydrographic boundaries. Time-series of size-based spatial TPL exponents also differ between hydrographically distinct basins.

5. These findings support the notion that TPL exponents contain ecological information, capturing community spatio-temporal dynamics as influenced by external drivers.

Introduction

A major challenge in ecology is condensing the complexity of ecosystem dynamics into quantifiable metrics. In 1961, Taylor posited that the variance in the

abundance of a population scales with the mean abundance of that population as a power law, such that:

$$\sigma^2 = \alpha\mu^{\beta}, \alpha > 0, \quad (1)$$

where $\sigma^2$is the variance in abundance of the population and μ is the mean abundance of the population, with the coefficient α and the scaling exponent β. His findings were based on empirical observations from a range of different organisms and became known as Taylor's power law (TPL). This relationship has since been verified in many more taxa and communities (e.g. Xu *et al.*, 2015; Döring *et al.*, 2015; Ramsayer *et al.* 2012), and even in non-ecological systems, where it is also known as fluctuation scaling (Eisler *et al.*, 2008).

Conceptually, TPL describes the level of aggregation between individuals in populations, captured by the scaling exponent, β, while the coefficient α is taken to be an artefact of sampling methodology (Taylor, 1961). If individuals are distributed randomly, then the Poisson distribution is approached, giving $\sigma^2 = \mu$, and therefore $\beta = 1$. An increasing β describes increasing heterogeneity beyond random (i.e. aggregation), whereas a decreasing β describes populations tending towards a uniform or more even distribution. The β term can therefore be taken as a descriptive measure of aggregation. If mean-variance pairs are calculated from abundances taken across space but at the same point in time, then β reflects the spatial aggregation of individuals, which we denote $\beta(s)$, and is known as spatial TPL. This can be interpreted as the degree of patchiness, with increasing $\beta(s)$ reflecting greater clustering in space. Conversely, if mean-variance pairs are estimated from abundances measured through time but at the same location then the temporal aggregation in the populations is described. This is referred to as temporal TPL, where the exponent, $\beta(t)$, can be taken as a measure of the magnitude of fluctuations in abundance of populations through time.

Beyond a purely descriptive use, there have been other practical applications of TPL in ecology. For instance, measures of $\beta(t)$ have been used to improve sampling regimes for bioassessments (Monaghan, 2015; Xu *et al.*, 2016). Reed & Hobbs (2004) and Pertoldi *et al.* (2008) used modified forms of $\beta(t)$ to explore extinction risk in small-sized populations. The residuals in temporal TPL have been proposed as a measure of stability in crop yields (Döring *et al.*, 2015) and similarly, the spatial heterogeneity of plants has also been described using residuals from spatial TPL regressions (Guan *et al.*, 2016).

The mechanism by which TPL emerges is, however, still heavily debated in the literature. Many theoretical models have been produced that seek to explain the emergence of TPL in ecological systems including those based on: density dependent (Perry 1994) or independent, stochastic population growth (Anderson *et al.*, 1982; Cohen *et al.*, 2013); reproductive covariance (Ballantyne & Kerkhoff, 2007); dispersal distance (Shi *et al.*, 2016); competition (Kilpatrick & Ives, 2003) or population synchrony (Cohen & Saitoh, 2016; Reuman *et al.,* 2017). Others argue that the ubiquity of TPL suggests less system specific causes such as data series length and sampling error (Kalyuzhny *et al.*, 2014) or statistical artefacts of system configuration (Xiao *et al.*, 2015). These theoretical models seek to explain TPL emergence with a typical exponent of $1 \leq \beta \leq 2$, as this is the typical range observed in empirical studies, however few offer widely applicable interpretations of variation in exponent values (but see Cohen *et al.* 2013 and Reuman *et al.,* 2017). Kilpatrick & Ives (2003) argued that the null expectation for $\beta(t)$ is a value of 2 due to the scaling between the mean and variance of random variables. Tokeshi (1995) illustrated graphically that, when estimating either $\beta(t)$ or $\beta(s)$, data will be constrained on the log-log plot between the hard upper bound of variance for a given mean that has a slope of 2 and a soft lower bound of

100 variance given the mean, the Poisson distribution, with a slope of 1, matching empirical
101 observation. However estimates are known to vary outside of these limits (Taylor *et al.*,
102 1980; Taylor & Woiwood, 1982) and, theoretically, any exponent value is feasible
103 (Cohen, 2014). Xiao *et al.* (2015) highlight the fact that, while TPL is statistically
104 inevitable, the exact form cannot be predicted on purely statistical grounds and
105 therefore may still contain ecological information.

106 Empirical data suggest that TPL exponents do contain ecologically relevant
107 information (Taylor & Woiwood, 1982; Lagrue *et al.*, 2015), however this is particularly
108 evidenced for fishes. A systematic reduction in $\beta(t)$ was found in fishes along gradients
109 of increasing connectivity and size of reefs, implying that fish species experience greater
110 temporal fluctuations in abundance on smaller, more isolated reefs, following known
111 patterns of recruitment (Mellin *et al.*, 2010). Analysis of larval survey data from
112 California revealed that the spatial heterogeneity of fish species, as measured by $\beta(s)$,
113 varied with both life history, decreasing with more "*K*-selected" traits, and fishing
114 pressure, increasing if the species was commercially targeted (Kuo *et al.,* 2016). These
115 studies suggest that both spatial and temporal TPL exponents, $\beta(t)$ and $\beta(s)$, could be
116 considered as potential ecological metrics as they appear to be sensitive enough to track
117 changes in temporal fluctuations and spatial patchiness of fish populations.

118 A key finding in both of the studies discussed above was the importance of body
119 size when determining sources of variation in $\beta(t)$ and $\beta(s)$ between species. Mellin *et*
120 *al.* (2010) found that the maximum length of a species explained 35% of the variation in
121 $\beta(t)$ alone whereas Kuo *et al.* (2016) found a strong negative linear relationship
122 between $\beta(s)$ and maximum body size, arguing that larger organisms are better able to
123 buffer environmental stresses.

Fish communities and aquatic systems are notably size structured where the size spectrum, the power law distribution of body sizes when size is considered at the individual-level, is commonly employed as an ecological metric (Kerr & Dickie, 2003; Gómez-Canchong *et al.,* 2013; Trebilco *et al.,* 2013). Further, body size is, in general, a key biological trait affecting almost all aspects of individual ecology (Peters 1983). Cohen *et al.* (2012) predicted that allometric scaling exists between body size and variance in abundance by combining TPL with estimates of population-level mean biomass. However another approach would be to parameterise TPL exponents by grouping individuals into classes of body size, rather than taxonomic groups, as is done with size spectra. If, as Kuo *et al.* (2016) suggested, heterogeneity due to environmental stresses are dependent on individual size and because smaller individuals are almost always more abundant than larger individuals, calculating TPL exponents as a function of body size rather than species may be more sensitive to detecting environmentally driven changes in spatial patchiness and temporal fluctuations.

Using one of the most spatially dense, long-term fish survey datasets available, the North Sea International Bottom Trawl Survey (NS-IBTS; ICES, 2015), we employ $\beta(t)$ and $\beta(s)$ as ecological metrics of temporal fluctuations and spatial patchiness respectively as applied to fish communities. We derive $\beta(t)$ and$\beta(s)$ at the community level (e.g. Grman *et al.,* 2010; Cohen *et al.,* 2016), allowing us to determine spatially explicit values of $\beta(t)$ and temporally explicit values of $\beta(s)$. We then determine the sensitivity of $\beta(t)$ and $\beta(s)$ by quantifying extreme values and testing whether these values are randomly distributed in relation to the external environment. Specifically, we test the hypothesis that fish community $\beta(t)$ increases with proximity to hydrographic boundaries, where interannual environmental variability is higher due to the lack of a dominant hydrographic regime (van Leeuwen *et al.*, 2015). We also test the hypothesis

149 that, over time, the community $\beta(s)$ differs between two hydrographically distinct
150 basins: the deep northern North Sea that is permanently stratified and the shallow
151 southern North Sea that is seasonally well-mixed (Heessen *et al.*, 2015; van Leeuwen *et*
152 *al.*, 2015). Finally, we test the hypothesis that both $\beta(t)$ and $\beta(s)$ are more sensitive
153 when individuals are considered by body size by comparing trends with hydrography in
154 exponents derived from groups of individual length classes with those derived from
155 groups by species.
156
157 **Materials and Methods**
158 The analytical workflow from survey data through to $\beta(t)$ and $\beta(s)$ calculations and
159 hypothesis testing is summarised as a schematic in Fig. 1, with numbered sections
160 expanded upon below.
161
162 *Data Sources and Processing (1)*
163 Fish community data from the ICES International Bottom Trawl Survey for the
164 North Sea (NS-IBTS) were sourced from DATRAS (http://www.ices.dk/marine-
165 data/data-portals/Pages/DATRAS.aspx - accessed 03/09/2015). The NS-IBTS is an
166 internationally coordinated survey originally conducted to estimate the distribution of
167 juvenile herring, *Clupea harengus,* in the North Sea, although it was quickly expanded to
168 target other species, notably round fish such as cod, *Gadus morhua.* The survey provides
169 abundance estimates as Catch Per Unit Effort (CPUE) for each species caught (all fish
170 and some invertebrate species of interest) binned into length classes within spatial
171 rectangles of 0.5° latitude by 1.0° longitude, with an approximate area of 30km^2, known
172 as subareas (ICES, 2015).

Data included in this study are limited to the years 1977 through to 2015, after the commencement of gear standardisation (GOV trawl with approximately 30 minute duration), although this was only fully adopted by all eight participating nations from 1983 and differences between rigging set-ups still remain (ICES, 2015). Further, data were limited to quarter one only, when survey cruises typically occur from mid January to mid February, to exclude seasonal differences in abundance (ICES, 2015). In total, the dataset used here contains over one million observations. All invertebrate records were removed and fish records of less than 60mm in length were excluded due to inefficient sampling within the trawl gear (Daan *et al.*, 2005). Length classes for all species were consolidated into 10mm bins, taxonomic identifications were corrected following Heessen *et al.* (2015) and subareas with fewer than 10 years of sampling were removed.

In order to assign subareas to the deep, northern basin or the shallow, southern basin, average depth was taken as the mean depth using ETOPO1 1arc-minute global relief model with a resolution of 1800 data points per subarea (Amante & Eakins, 2009). In the North Sea, the 50m-depth contour approximately demarcates the difference between deep, permanently stratified and shallow, seasonally well-mixed waters (Heessen *et al.,* 2015). Accordingly, subareas with average depth ≤ 50m were assigned to the shallow basin whereas those with average depths >50m were assigned to the deep basin (see Fig. 2a).

Mean-Variance Calculations (2):

We applied the following argument to calculate the mean and variance in abundance. Let $x_{s,t,p,l}$ denote the abundance of species p of length class l sampled in subarea s in year t. Individuals were grouped into species and abundances pooled across length classes, such that the abundance for species p sampled in subarea s in

year t is $x_{s,t,p} = \sum_{l=1}^{n_{s,t,p}} x_{s,t,p,l}$ where $n_{s,t,p}$ is the number of length classes for species p sampled in subarea s in year t. Separately, individuals were grouped into length classes and abundances pooled across species, such that for length class l, $x_{s,t,l} = \sum_{p=1}^{n_{s,t,l}} x_{s,t,p,l}$ where $n_{s,t,l}$ is the number of species.

For each subarea, the mean abundance of each species was calculated through time, $\bar{x}(t)_{s,p} = \frac{1}{n_{s,p}} \sum_{t=1}^{n_{s,p}} x_{s,t,p}$, and similarly the variance in abundance through time for each species, denoted $s^2(t)_{s,p}$ where $n_{s,p}$ is the number of years sampled in that subarea for species p (left-hand side of part 2, Fig. 1). Note that $n_{s,p}$ will be the same for all species within subarea s. As time-series length can influence temporal TPL parameters (Kalyuzhny *et al.*, 2014), we limited subareas to those with at least 30 years of sampling ($n_{s,p} \geq 30$). Further, species with fewer than 10 years of presence (i.e. less than 10 non-zero abundance records) within a subarea were excluded so that transient species, which cause zero-inflation of variance, were not included in the community TPL parameterisation. Years of absence for species within a subarea were then assigned an abundance value of zero. The temporal mean and variance of abundance were calculated using the same method for each length class in each subarea giving $\bar{x}(t)_{s,l}$ and $s^2(t)_{s,l}$ where $n_{s,l} = n_{s,p}$.

Spatial mean-variances pairs were calculated for each year across subareas within the deep and shallow basins separately for each species. Typically, zero data in spatial TPL analyses are excluded *a priori,* however this causes selection bias in data where zero abundance can be valid, potentially influencing the estimates of α and β (Jørgensen *et al.*, 2011). Here, this was accounted for by constructing a feasible habitat area within each basin for each species / length class (blue-background subareas in abundance maps on the right-hand side of Fig. 1). This was done by taking the overlap

of the subareas sampled within the basin during any one year and all the subareas that the species (or length class) had occurred in within that basin over the whole time period.

The spatial mean is then given as $\bar{x}(s_z)_{t,p} = \frac{1}{n^z_{t,p}} \sum_{s=1}^{n^z_{t,p}} x_{s_z,t,p}$, where the subscript z denotes the basin ($z = d$ for deep and $z = sh$ for shallow) and $n^z_{t,p}$ is the number of subareas within the feasible habitat area for species p in basin z for year t. Note that $n^z_{t,p}$ will be unique for each species and may differ between years as the number of subareas sampled in each year can vary. Absences within feasible habitat areas were assigned zero abundance. The spatial variance was similarly calculated, denoted as $s^2(s_z)_{t,p}$. Here, we limited species to those present within at least five subareas (at least five non-zero abundance records) for any given year within a feasible habitat area of at least 25 subareas to exclude vagrants within the community and prevent zero inflation of variance. Using the same method, the spatial mean and variance of abundance were calculated for each length class in each year for each basin giving $\bar{x}(s_z)_{t,l}$ and $s^2(s_z)_{t,l}$.

TPL parameterisation (3):

From equation 1, it follows that the TPL exponent and coefficient can be estimated from the linear relationship of the logarithms using sample data:

$$\log(s^2) = \log(\hat{\alpha}) + \hat{\beta} \log(\bar{x}) + \epsilon, \quad \alpha > 0, \tag{2}$$

where ϵ is the residual error, with the form of TPL estimated depending upon whether temporal or spatial mean-variance pairs are used.

For each subarea, we estimated the temporal TPL (left-hand side of Fig. 1) for the community of individuals grouped by species, with the exponent denoted as $\hat{\beta}(t,p)_s$, using ordinary least squares linear regression (OLS) on the logarithmically transformed

$\bar{x}(t)_{s,p}$ and $s^2(t)_{s,p}$. We used base 10 logarithms although the base value is arbitrary for estimating β. We assigned equal weighting to mean-variance pairs as $n_{s,p}$ is the same for each species. We used the same approach to estimate the exponent when groups were defined as length classes, giving $\hat{\beta}(t, l)_s$.

For each year, the spatial TPL exponent (right-hand side of Fig. 1) was calculated separately for the deep and shallow basins using OLS on the logarithmically transformed means and variances, giving $\hat{\beta}(s_d, p)_t$ and $\hat{\beta}(s_{sh}, p)_t$ respectively for the species-based community. As the residual error, $\epsilon^z_{t,p}$, is approximately inversely proportional to the degrees of freedom used to estimate the means and variances (Perry, 1981; Jørgensen *et al.*, 2011) and here $n^z_{t,p}$ is unique for each species, we assigned weights of $n^z_{t,p} - 1$ to each mean-variance pair. The same method was applied to estimate the spatial TPL exponents for the size-based community, giving $\hat{\beta}(s_d, l)_t$ and $\hat{\beta}(s_{sh}, l)_t$.

To ensure that any observed trends were not an artefact of the statistical method used to parameterise TPL, we separately estimated all TPL exponents using the Siegel repeated medians method for linear regression (SM, Siegel 1982), a method that is highly robust to the influence of outliers (breakdown point of 50%, *ca.* 0% for OLS). For a set of *N* points (X_i, Y_i), SRM estimates the slope of the linear relationship $Y = a + bX$ as

$$\hat{b} = \underset{i}{Median}\left\{\underset{j \neq i}{Median} Slope(i, j)\right\} \quad (3)$$

where $Slope(i, j) = \frac{Y_j - Y_i}{X_j - X_i}$. Essentially, for each individual data point, this approach computes individual pairwise slopes with all other data points (excluding itself), from which the median is taken. The slope of the linear relationship is then taken to be the

median of *N* median slopes. SRM makes no assumptions about the error distribution of the residuals and takes equal weighting for pairs of data points.

Spatial and temporal trends with hydrography (4):

We explored spatial trends in the temporal TPL exponents (left-hand side of Fig. 1) by first testing whether estimated $\hat{\beta}(t,p)_s$ and $\hat{\beta}(t,l)_s$ for each subarea had a value that was extreme compared to that expected at random given the data $x_{s,t,p}$ and $x_{s,t,l}$ respectively. We employed the "feasible set" approach following Xiao *et al.* (2015), constructing a distribution of random temporal TPL exponents for each subarea given the data, conducted separately for groups by species and by length class. For each of 10000 permutations for species groupings, pairs of $\bar{x}(t)_{s,p}$ and $s^2(t)_{s,p}$ were randomly re-ordered across all species, *p,* and subareas, *s*, giving a random configuration of the data. Temporal TPL exponents were then calculated following the methods described above (both OLS and SRM methods separately), which we denote $\hat{\beta}(t,p)_s^r$, where the *r* superscript signifies that it is the random distribution from 10000 feasible set permutations. This approach maintains the same $n_{s,p}$ for each subarea and we permuted at the level of mean-variance pairs to avoid erroneous, ecologically implausible abundance structures. Confidence intervals at the 95% level were then constructed separately for each subarea by numerically integrating over $\hat{\beta}(t,p)_s^r$. This was repeated for groups by length class producing $\hat{\beta}(t,l)_s^r$ and associated confidence intervals. The *in situ,* empirical estimates of $\hat{\beta}(t,p)_s$ and $\hat{\beta}(t,l)_s$ were then tested against their confidence intervals and grouping methods compared, with estimates falling outside of their intervals suggesting that such values were unlikely to be generated by random processes alone for those subareas.

To test for patterns with hydrography, the spatial distribution of $\hat{\beta}(t,p)_s$ and $\hat{\beta}(t,l)_s$ were modelled as a linear function of their proximity to the nearest hydrographic boundary. Boundaries were taken as the subareas that contained: the 500m depth contour separating the North Sea from the Atlantic drift current; the 55°45'N line running between Denmark and Sweden separating the North Sea from the Baltic Sea; a straight line between Dover, UK, and Calais, France, separating the North Sea from the English Channel and the 50m depth contour from Oslofjord, Norway, to Scarborough, UK, which approximately demarcates the transition between the deep, permanently stratified waters and the shallow, seasonally well-mixed waters (Heessen *et al.*, 2015; van Leeuwen *et al.*, 2015). Subareas were assigned a proximity category of either "on", "adjacent to", or "distant from", see Fig. 2b.

For temporal trends in the spatial TPL exponents, we similarly tested for extreme values in $\hat{\beta}(s_z,p)_t$ and $\hat{\beta}(s_z,l)_t$ using the feasible set approach. We generated $\hat{\beta}(s_z,p)_t^r$ and $\hat{\beta}(s_z,l)_t^r$ by randomly re-ordering spatial mean-variance pairs across both deep and shallow basins prior to estimating the spatial TPL exponents separately for each basin. We carried forward $n_{t,p}^z$ and $n_{t,l}^z$ values with their mean-variance pairs for weighting in OLS. Confidence intervals were constructed at the 95% level and years whose empirical values fell outside of this range identified. Differences between the two hydrographically distinct basins were identified by constructing time-series and comparing the overlap in $\hat{\beta}(s_z,p)_t$ and $\hat{\beta}(s_z,l)_t$ estimates, using the standard errors of the slopes for the OLS method and the median absolute deviation (MAD) for the SRM method to estimate 95% confidence intervals, coupled with paired t-tests.

All analyses were conducted in R 3.3.2 (R Core Team, 2016), utilising the packages: "plyr" (Wickham, 2011); "data.table" (Dowle & Srinivasan, 2017); and "mblm"

(Komsta 2013). Map production was done utilising the package "maps" (Brownrigg *et al.,* 2017).

Results

Across all formulations, we calculated a total of 416 $\hat{\beta}$'s, each being estimated using two separate regression methods. For the OLS method, for which p-values were calculated, all $\hat{\beta}$'s showed a significant log-log linear relationship at the p = 0.05 level. A summary of the number of observations, r-squared values and orders of magnitude spanned by the regressions can be found in table 1. An example of the relationship between mean abundance, variance of abundance and body size used to calculate $\hat{\beta}(t,l)_s$ is shown in Fig. 3 (all individual TPL plots can be found in the Supplementary).

Temporal TPL

Maps of $\hat{\beta}(t,p)_s$ and $\hat{\beta}(t,l)_s$ are shown in Fig. 4, covering a total of 169 subareas in the North Sea. Values of $\hat{\beta}(t,p)_s$ ranged from 1.80 to 2.09 with a mean of 1.93 with only 3 subareas having values that fell outside their confidence intervals. Values of $\hat{\beta}(t,l)_s$ had a larger range from 1.64 to 2.21 with a mean of 1.98, with many more exponents falling outside their confidence intervals – 31 in total, see Fig. 4b. Further, values of $\hat{\beta}(t,l)_s$ systematically decreased with decreasing proximity to hydrographic boundaries ($F_{1,167} = 40.0$, $p < 0.001$), whereas values of $\hat{\beta}(t,p)_s$ showed no trend with proximity ($F_{1,167} = 0.975$, $p = 0.325$), see Fig. 5. Similar results were obtained using SRM regression; see the Supplementary for figures.

Spatial TPL

Time series of $\hat{\beta}(s_d, p)_t$ and $\hat{\beta}(s_{sh}, p)_t$, spanning 39 years are shown in Fig. 6. In total, only one year had a value outside its confidence intervals for $\hat{\beta}(s_d, p)_t$ and only three years for $\hat{\beta}(s_{sh}, p)_t$. The spatial TPL time series for the deep and shallow basins were generally similar over the whole period, overlapping for the majority of years and with no mean difference between $\hat{\beta}(s_d, p)_t$ and $\hat{\beta}(s_{sh}, p)_t$ (t_{38} = -0.537, p = 0.594). Conversely, the time series of $\hat{\beta}(s_d, l)_t$ and $\hat{\beta}(s_{sh}, l)_t$ had 19 and 13 years respectively where values fell outside of their confidence intervals. The majority of these were lower than expected for the deep basin (18 out of 19) but higher than expected for the shallow basin (11 out of 13). The two time series show considerable divergence over much of the sampling period; with $\hat{\beta}(s_d, l)_t$ being significantly lower on average compared to $\hat{\beta}(s_{sh}, l)_t$ (t_{38} = 6.01, p < 0.001). As with temporal TPL, qualitatively similar results were obtained when using SRM regression to estimate spatial TPL exponents; see the Supplementary for figure and associated statistics.

Discussion

Ecosystems are both complex and dynamic, making it challenging to characterise and quantify responses in ecosystem structure to external conditions. Taylor's Power Law has been proposed as a metric describing the extent of aggregation of organisms within systems. We empirically tested whether the aggregation of organisms by species and across size classes within a community, as measured by Taylor's Power Law exponents, varied systematically in response to external environmental conditions. Using a long-term and spatially dense community dataset, we have shown that:

(1) Within the North Sea fish community, TPL exponents largely fall between $1<\beta<2$, agreeing with previous empirical work.

(2) We found systematic differences in both spatial and temporal TPL exponents within the North Sea associated with regional hydrography and therefore the *in situ* environment, with high values of β typically associated with more dynamic hydrographic conditions.

(3) Systematic relationships between TPL exponents and the external environment were only apparent when mean-variance pairs were calculated from body size rather than species-level data (Figs. 4 & 6).

Here we infer that systematic variations in TPL exponents are related to the extent of variability (dynamism) in external hydrographic conditions and therefore capture ecological information, providing practical as well as theoretical applications of TPL.

For temporal TPL we found higher exponents, implying relatively higher temporal variance in abundance at smaller body sizes, in more hydrographically dynamic areas. Notably, high estimates of $\beta(t)$ tracked the 50m-depth contour that separates the two basins within the North Sea, see Fig. 3, an area where a lack of a dominant hydrographic regime between years imparts higher interannual variability at these localities (van Leeuwen *et al.*, 2015). Variability within the environment is a key component of models that seek to explain the emergence of temporal TPL, for example, Saitoh & Cohen (2018) showed a strong positive linear relationship between modeled environmental variability and $\beta(t)$ in their simulations of vole populations. The results presented here provide empirical evidence that has previously been lacking for such a key relationship utilised in simulation modeling of TPL. While we have successfully used TPL exponents to demonstrate differences in temporal fluctuations between subareas, identifying specific environmental drivers influencing these differences is much more difficult.

Of particular pertinence to the fish data examined here is the effect of fishing pressure on community structuring. It has long been known that fishing can amplify the magnitude of temporal fluctuations in fish stocks (Shelton & Mangel, 2011; Essington *et al.,* 2015) and given that the North Sea has some of the highest fishing pressures in the world (Amoroso et al. 2018), one might expect there to be a strong link between size-selective fishing pressure and temporal TPL. Although not explicitly tested for due to additional complexities in the available fishing effort data, we observe no obvious correlations between the spatial distribution in $\beta(t)$ and the distribution in fishing effort or gear type (Jennings *et al.*, 1999). Instead, we find that the distribution of abundance within size classes is more variable through time at locations at boundaries between areas of contrasting but dynamic environmental conditions. It is certainly possible that high fishing pressure across the North Sea enhances the effect of environmental dynamism on community abundances, but we do not have data to test this.

Recently, research on more specific sources of variability in $\beta(s)$ has focused on the spatial synchrony of populations, which is the degree to which abundances between geographically separate populations are correlated (Cohen & Saitoh, 2016; Reuman *et al*., 2017). High spatial correlation results in a reduction in the expected variance for a given mean abundance, and therefore increased spatial synchrony typically manifests as a reduction in the spatial TPL exponent (Reuman *et al.*, 2017). Dispersal mechanisms can result in spatial synchrony, however typically spatial synchrony can be attributed to spatially correlated environments, known as the Moran effect (Moran 1953, Koenig & Liebhold 2016), which has been shown in reef fishes (Cheal *et al.*, 2007).

Our results showed, on average, a reduced $\beta(s)$ at the community level in the deep, permanently stratified basin compared to the shallow, seasonally well-mixed

basin, which could be explained by a more spatially correlated environment in the deeper northern North Sea. However, the time series of $\beta(s)$ exhibited alternating periods of divergence and tight coupling between the two basins, suggesting greater complexity in the drivers of $\beta(s)$ than a static Moran effect. Indeed, the reducing effects of spatial synchrony can be masked by other drivers of variability, as has been shown for chlorophyll-a data (Reuman *et al.*, 2017). Interestingly, recent theoretical work suggests that fishing pressures may in fact change the degree of spatial synchrony within harvested populations (Engen *et al.*, 2018) and therefore asymmetric fishing practices cannot be excluded as a potential driver of trends in $\beta(s)$. Fishing methods vary between the northern and southern basins in the North Sea (Jennings *et al.,* 1999), reflecting differences in water depth and community composition. We are unable to determine therefore whether the observed increased patchiness in the southern basin, inferred by a higher $\beta(s)$ time-series, reflects spatial differences in hydrology, community composition, fishing effort or some combination of all three.

The observed patterns in $\beta(t)$ and $\beta(s)$ only held when communities were considered as consisting of individuals grouped into different classes of body size. The scaling of mean abundance with individual body size, known as the size spectrum (Kerr & Dickie, 2001), has long been considered an ecosystem metric. In particular, it is often used in reference to size-selective fishing, which causes a truncation in abundances of larger body sizes and a resultant increase in the magnitude of scaling exponent (e.g. Daan *et al.,* 2005). By grouping individuals by body size, the resultant $\beta(t)$ and $\beta(s)$ estimates quantify the variability in the distribution of biomass by body size in the community (i.e. the size spectrum) either through time (as the magnitude of temporal fluctuations) or across space (degree of patchiness in the spatial distribution) respectively. The relationship between mean abundance, variance in abundance and

437 body size is demonstrated in Fig. 3. Scaling of variance in abundance with mean body
438 size across the range of TPL exponents exhibited in the North Sea is shown in Figure 7.
439 Changes in the TPL exponent result in greater relative changes in the variability of
440 abundance at smaller body sizes, which is in agreement with the findings of Mellin et al.
441 (2010) and Kuo et al., (2016) who showed the importance of body size in β(t) and β(s)
442 respectively at the species-level. Community TPL therefore provides complementary
443 information to that of the biomass size spectrum regarding the variability of community
444 structure in time and space. Our results suggest that external environmental drivers
445 systematically influence ecosystem structural dynamics as coded by community TPL
446 exponents.
447 We recognise that trawl sampling introduces systematic biases. Notably, very
448 small and very large body sizes are under-represented, which is important given that
449 our results show size-associated trends. Similarly, different species also have different
450 rates of catchability (ICES, 2015). Nevertheless a broadly consistent sampling approach
451 was used throughout the survey series; therefore data are comparable across time and
452 space. To further reduce the potential for gear selection biases in the dataset, we
453 excluded *a priori* very small body sizes (<60mm) and extremely rare observations of
454 species and body sizes. We chose the NS-IBTS dataset in order to maximise the signal to
455 noise ratio when considering environmental correlates of TPL. The potential for
456 recovering signal was increased by a dataset containing more than one million
457 observations sampled using a relatively consistent methodology across known
458 gradients of environmental conditions. Further, noise due to error in TPL estimates was
459 reduced by sampling a relatively large range of body sizes, spanning up to two orders of
460 magnitude by length from a total of 147 species, resulting in relatively well-constrained
461 regression models.

462 Variations in community structure in time and space are more than simply
463 absolute changes in abundance either as a function of taxonomy or body size (Cohen,
464 2014). Ecosystems are notably complex, however current theoretical work is outpacing
465 our ability to ground-truth predictions. Metrics that can empirically capture patterns of
466 ecosystem structure beyond simple changes in abundance are therefore required in
467 order to test ecological theory as well as monitor these important systems. We show
468 that TPL exponents efficiently capture differences in the variance of abundance or
469 biomass across size spectra (or taxonomic groups) in the North Sea fish community and
470 that the differences can be related to ecological, environmental or anthropogenic
471 drivers. Coupled with the versatility of how it can be estimated (across space, through
472 time, at the species or community level etc.), we argue Taylor's Power Law is a
473 promising candidate for the development of new ecosystem metrics.
474
475 **Acknowledgements**
476 This work was funded by a NERC SPITFIRE PhD studentship (award number
477 1498909). We would like to thank the contribution of all scientists and colleagues
478 working on the collection and processing of data within ICES. The authors declare no
479 conflict of interest with regard to the work presented here.
480
481 **References:**
482 Amante, C. and Eakins, B. W. (2009) ETOPO1 1 arc-minute global relief model:
483 procedures, data sources and analysis. NOAA Technical Memorandum NESDIS
484 NGDC-24., National Geophysical Data Center, NOAA. Doi:10.7289/V5C8276M
485 [accessed 23/07/2015]

Amoroso, R. O., Pitcherb, C. R., Rijnsdorp, A. D>, McConnaughey, R. A., Parma, A. M., Suuronen, P., Eigaard, O. R. *et al.* (2018) Bottom trawling fishing footprints on the world's continental shelves. *Proceedings of the National Academy of Sciences*, doi:10.1073/pnas.1802379115

Anderson, R. M., Gordon, D. M., Crawley, M. J. and Hassell, M. P. (1982) Variability in the abundance of animal and plant species. *Nature,* 296, 245-248

Ballantyne IV, F. & Kerkhoff A. J. (2007) The observed range for temporal mean-variance scaling exponents can be explained by reproductive correlation. *Oikos,* 116, 174-180

Brownrigg R. Minka, T. P. and Deckmyn, A. (2017). maps: Draw Geographical Maps. R package version 3.2.0. Original S code by Richard A. Becker, Allan R. Wilks., https://CRAN.R-project.org/package=maps

Cheal, A. J., Delean, S., Sweatman, H., & Thompson, A. A. (2007). Spatial synchrony in coral reef fish populations and the influence of climate. *Ecology*, *88*(1), 158-169.

Cohen, J. E., Xu, M. and Schuster, W. S. F. (2012) Allometric scaling of population variance with mean body size is predicted from Taylor's law and density-mass allometry. *Proceedings of the National Academy of Sciences*, 109, 15829-15834

Cohen, J. E., Xu, M. and Schuster, W. S. F. (2013) Stochastic multiplicative population growth predicts and interprets Taylor's power law of fluctuation scaling. *Proceedings of the Royal Society London B,* 280, 20122955

Cohen, J. E. (2014) Taylor's law and abrupt biotic change in a smoothly changing environment. *Theoretical Ecology,* 7, 77-86

Cohen, J. E., Lia, J., Coomes, D. A. and Allen, R. B. (2016) Taylor's law and related allometric power laws in New Zealand mountain beech forests: the roles of space, time and environment. *Oikos*, 125, 1342-1357

511 Cohen, J. E. and Saitoh, T. (2016) Population dynamics, synchrony and environmental
512 quality of Hokkaido voles lead to temporal and spatial Taylor's laws. *Ecology*,
513 97(12), 3402-3413
514 Daan, N., Gislason, H., Pope, J. G. and Rice, J. C. (2005) Changes in the North Sea fish
515 community: evidence of indirect effects of fishing? *ICES Journal of Marine Science,*
516 62, 177-188
517 Döring, T. F., Knapp, S. and Cohen, J. E. (2015) Taylor's power law and the stability of
518 crop yields. *Field Crops Research,* 183, 294-302
519 Dowle, M. and Srinivasan A. (2017). data.table: Extension of `data.frame`. R package
520 version 1.10.4-3. https://CRAN.R-project.org/package=data.table
521 Eisler, Z., Bartos, I. and Kertész J. (2008) Fluctuation scaling in complex systems:
522 Taylor's law and beyond[1]. *Advances in Physics.,* 57, 89-142
523 Engen, S., Cao, F. J. & Sæther, B.-E. (2018) The effect of harvesting on the spatial
524 synchrony of population fluctuations. *Theoretical Population Biology*, 123, 28-34
525 Essington, T. E., Moriarty, P. E., Froehlich, H. E., Hodgson, E. E., Koehn, L. E., Oken, K. L.,
526 Siple, M. C., *et al.* (2015). Fishing amplifies forage fish population
527 collapses. *Proceedings of the National Academy of Sciences*, 201422020.
528 Gómez-Cachong, P., Blanco, J. M. and Quiñones R. A. (2013) On the use of biomass size
529 spectra linear adjustments to design ecosystem indicators. *Scientia Marina,* 77,
530 257-268
531 Grman, E., Lau, J. A., Schoolmaster Jr., D. R. and Gross, K. L. (2010) Mechanisms
532 contributing to stability in ecosystem function depend on the environmental
533 context. *Ecology Letters,* 13, 1400-1410

534 Guan, Q., Chen, J., Wei, Z., Wang, Y., Shiyomi, M. and Yang, Y. (2016) Analyzing the spatial
535 heterogeneity of number of plant individuals in grassland community by using
536 power law model. *Ecological Modelling.,* 320, 316-321
537 Heessen, H. J. L., Daan, N. and Ellis, J. R. (2015) *Fish atlas of the Celtic Sea, North Sea, and*
538 *Baltic Sea.* Wageningen Academic Publishers, The Netherlands
539 ICES (2015) Manual for the international bottom trawl surveys. Series of ICES survey
540 protocols SISP 10 – IBTS IX. 86 pp.
541 Jennings, S., Alvsvåg, J., Cotter, A. J. R., Ehrich, S., Greenstreet, S. P. R., Jarre-Teichmann,
542 A., Mergardt, N, *et al.* (1999). Fishing effects in northeast Atlantic shelf seas:
543 patterns in fishing effort, diversity and community structure. III. International
544 trawling effort in the North Sea: an analysis of spatial and temporal
545 trends. *Fisheries Research*, *40*, 125-134.
546 Jennings, S., Greenstreet, S., Hill, L., Piet, G., Pinnegar, J., & Warr, K. (2002) Long-term
547 trends in the trophic structure of the North Sea fish community: evidence from
548 stable-isotope analysis, size-spectra and community metrics. *Marine Biology*,
549 141, 1085–1097.
550 Jørgensen, B., Demétrio, C. G. B., Kristensen, E., Banta, G. T., Petersen, H. C., Delefosse, M.
551 (2011) Bias-corrected Pearson estimating functions for Taylor's power law
552 applied to benthic macrofauna. *Statistics and Probability Letters*, 81, 749-758
553 Kalyuzhny, M., Schreiber, Y., Chocron, R., Flather, C. H., Kadmon, R., Kessler, D. A. and
554 Shnerb, N. M. (2014) Temporal fluctuation scaling in populations and
555 communities. *Ecology,* 95, 1701-1709
556 Kerr, S. R. and Dickie, L. M. (2001) *The biomass spectrum: a predator-prey theory of*
557 *aquatic production.* Columbia University Press

558 Kilpatrick,, A. M. and Ives, A. R. (2003) Species interactions can explain Taylor's power
559 law for ecological time series. *Nature,* 422, 65-68
560 Koenig, W. D. & Liebhold, A. M. (2016) Temporally increasing spatial synchrony of North
561 American temperature and bird populations. *Nature Climate Change*, 6, 614-618
562 Komsta, L. (2013). mblm: Median-Based Linear Models. R package version 0.12.
563 https://CRAN.R-project.org/package=mblm
564 Kuo, T., Mandal, S., Yamauchi, A. and Hsieh, C. (2016) Life history traits and exploitation
565 affect the spatial mean-variance relationship in fish abundance. *Ecology*, 97(5),
566 1251-1259
567 Lagrue, C., Poulin, R. and Cohen, J. E. (2015) Parasitism alters three power laws of
568 scaling in a metazoan community: Taylor's law, density-mass allometry, and
569 variance-mass allometry. *Proceedings of the National Academy of Sciences*, 112,
570 1791-1796
571 Mellin, C., Huchery, C., Caley, M. J., Meekan, M. G. and Bradshaw, C. J. A. (2010) Reef size
572 and isolation determine the temporal stability of coral reef fish populations.
573 *Ecology,* 91(11), 3138-3145
574 Monaghan, K. A. (2015) Taylor's law improves the accuracy of bioassessment; an
575 example for freshwater macroinvertebrates. *Hydrobiologia,* 760, 91-103
576 Moran, P.A.P. (1953) The statistical analysis of the Canadian lynx cycle: II
577 Synchronisation and meteorology. *Australian Journal of Zoology,* 1:291–298.
578 Perry, J. N. (1981) Taylor's power law for dependence of variance on mean in animal
579 populations. *Journal of Applied Statistics,* 30(3), 254-263
580 Perry, J. N. (1994) Chaotic dynamics can generate Taylor's power law. *Proceedings of the*
581 *Royal Society London B,* 257, 221-226

582 Pertoldi, C., Bach, L. A. and Loeschcke, V. (2008) On the brink between extinction and
583 persistence. *Biology Direct,* 3(1), 47
584 Peters, R. H. (1983) *The ecological implications of body size.* University Press, Cambridge,
585 UK
586 R Core Team (2016). R: A language and environment for statistical computing. R
587 Foundation for Statistical Computing, Vienna, Austria. URL https://www.R-
588 project.org/.
589 Ramsayer, J., Fellous, S., Cohen, J. E. and Hochberg, M. E. (2012) Taylor's law holds in
590 experimental bacterial populations but competition does not influence the slope.
591 *Biology Letters,* 8, 316-319
592 Reed, D. H. and Hobbs, G. R. (2004) The relationship between population size and the
593 temporal variability in population size. *Animal Conservation,* 7, 1-8
594 Reuman, D. C., Zhao, L., Sheppard, L. W., Reid, P. C. and Cohen, J. E. (2017) Synchrony
595 affects Taylor's law in theory and data. *Proceedings of the National Academy of*
596 *Sciences*, 114, 6788-6793
597 Saitoh, T., & Cohen, J. E. (2018). Environmental variability and density dependence in
598 the temporal Taylor's law. *Ecological Modelling*, *387*, 134-143.
599 Shelton, A. O., & Mangel, M. (2011). Fluctuations of fish populations and the magnifying
600 effects of fishing. *Proceedings of the National Academy of Sciences*, *108*(17), 7075-
601 7080.
602 Shi, P., Sandhu, H. S. and Reddy, G. V. P. (2016) Dispersal distance determines the
603 exponent of the spatial Taylor's power law. *Ecological Modelling,* 335, 48-53
604 Siegel, A. F. (1982) Robust regression using repeated medians. *Biometrika,* 69, 242-
605 244Taylor, L. R. (1961) Aggregation, variance and the mean. *Nature,* 189, 732-735

606 Taylor, L. R., Woiwod, I. P. and Perry, J. N. (1980) Variance and the large scale spatial
607 stability of aphids, moths and birds. *Journal of Animal Ecology,* 49, 831-854
608 Taylor, L. R. and Woiwod, I. P. (1982) Comparative synoptic dynamics. I. Relationships
609 between inter- and intra-specific spatial and temporal variance/mean population
610 parameters. *Journal of Animal Ecology,* 51, 879-906
611 Tokeshi, M. (1995) On the mathematical basis of the variance-mean power relationship.
612 *Researches on Population Ecology,* 37, 43-48
613 Trebilco, R., Baum, J. K., Salomon, A. K. and Dulvy, N. K. (2013) Ecoseystem ecology: size-
614 based constraints on the pyramids of life. *Trends in Ecology & volution*, 28, 423-
615 431.
616 van Leeuwen, S., Tett, P., Mills, D. and van der Molen, J. (2015) Stratified and
617 nonstratified areas in the North Sea: Long-term variability and biological and
618 policy implications. *Journal of Geophysical Research: Oceans,* 120, 4670-4686
619 Wickham H. (2011). The Split-Apply-Combine Strategy for Data Analysis. *Journal of*
620 *Statistical Software*, 40, 1-29
621 Xiao, X., Locey, K. and White, E. P. (2015) A process-independent explanation for the
622 general form of Taylor's law. *The American Naturalist,* 186(2), 51-60
623 Xu, M., William, S. F. and Cohen, J. E. (2015) Robustness of Taylor's law under spatial
624 hierarchical groupings of forest tree samples. *Population Ecology,* 57(1), 93-103
625 Xu, M., Kolding, J. and Cohen, J. E. (2016) Taylor's power law and fixed-precision
626 sampling: Application to abundance of fish sampled by gillnets in an African lake.
627 *Canadian Journal of Fisheries and Aquatic Sciences,* 74, 87-100
628
629 **Figures and Tables**

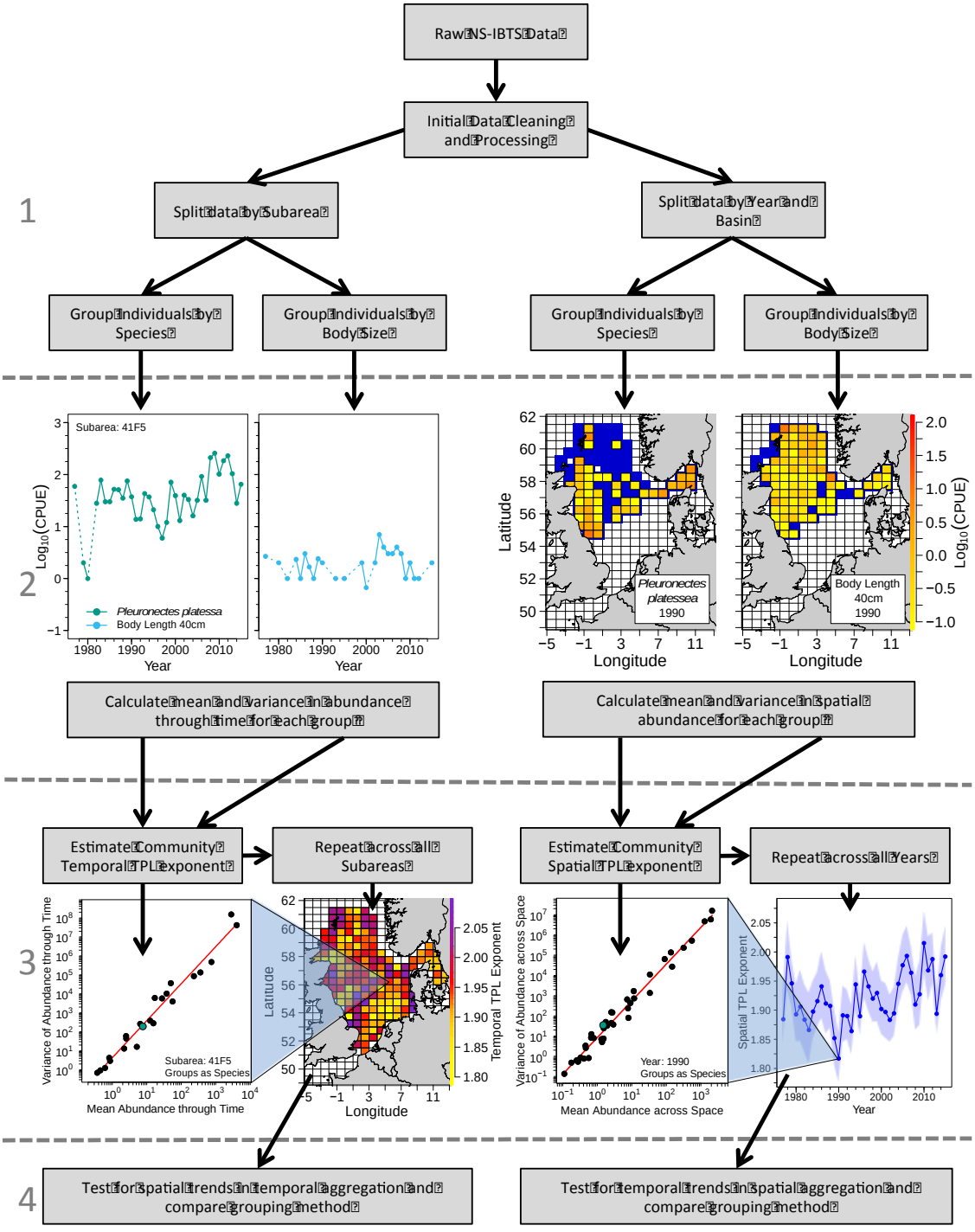

Figure 1:

Schematic diagram illustrating the progression from data acquisition to construction of maps and time-series of TPL exponents. Methodology is split into 4 sections that are described in greater detail in the text. 1: Data sources and processing. 2: Mean-variance calculations. Dashed lines indicate years with zero abundance. Blue

636 subareas in abundance maps indicate feasible habitat area with zero abundance. 3: TPL
637 parameterisation, and 4: Spatial and temporal trends with hydrography. Note that
638 CPUE, mean abundance and variance in abundance axes are on logarithmic scales.
639
640

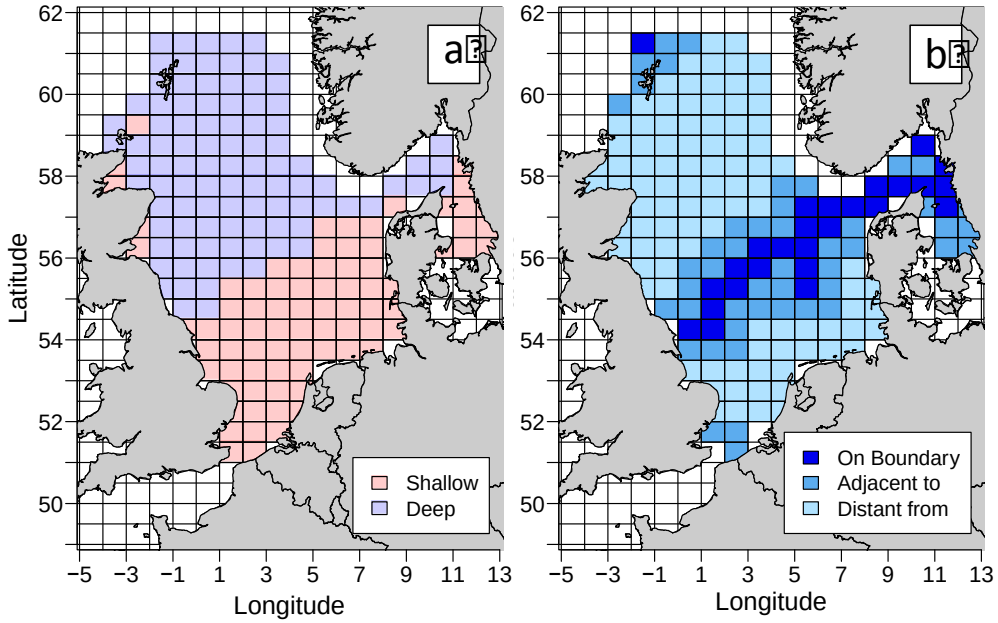

641
642 *Figure 2:*
643 Map of deep (>50m) and shallow (≤ 50m) subareas in the North Sea (a) and a map of
644 subarea assignment to proximity of hydrographic boundaries (b).
645
646

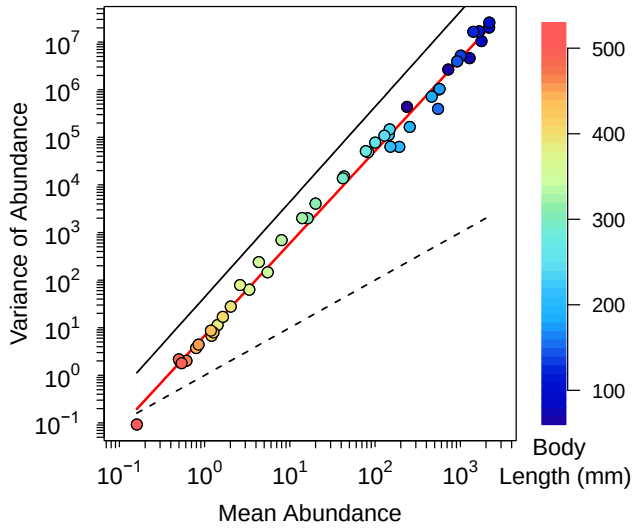

Figure 3:

An example of $\hat{\beta}(t,l)_s$ (temporal TPL by length class), visualised as the slope of the least-squares log-log linear regression (solid red line) between the mean and variance in abundance through time for the subarea "37F7". Solid and dashed black lines show the hard upper bound and soft lower bound of variance given the mean following Tokeshi (1995). Data points are coloured based on size. The smaller and larger size classes occupy the extremes of mean abundance and so are more influential in TPL parameter estimation, however variance at low mean abundances (larger size classes) is heavily bounded which limits leverage. Note the base 10 logarithmic scale.

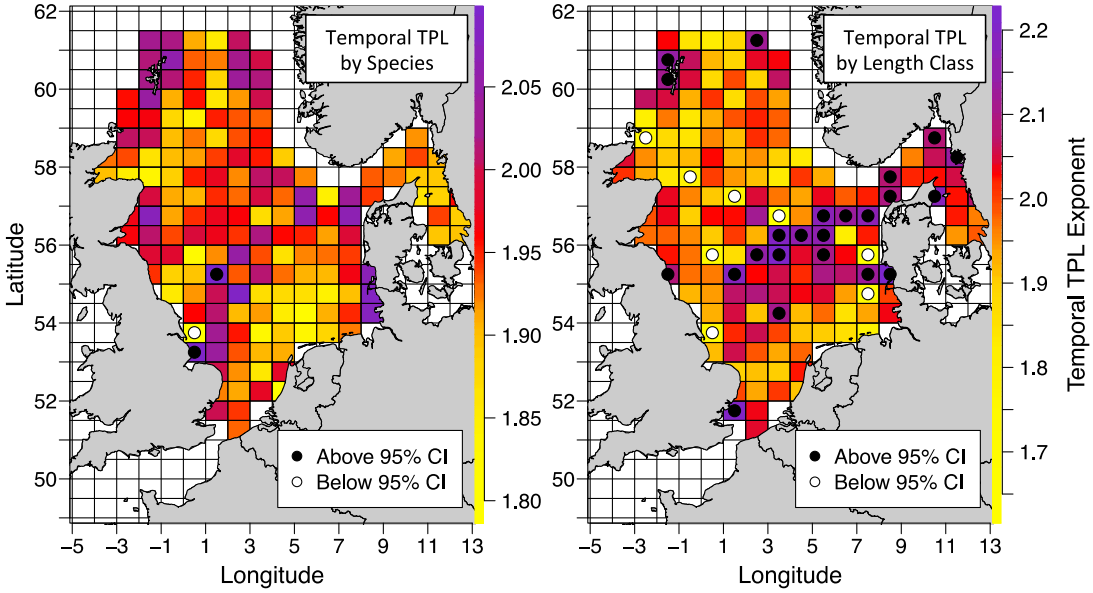

657

658 *Figure 4:*

659 Maps of $\hat{\beta}(t,p)_s$ (left hand side) and $\hat{\beta}(t,l)_s$ (right hand side) estimates for the

660 benthic fish community within 169 subareas across the North Sea (a and b

661 respectively). Subareas with exponent estimates either above or below the 95%

662 confidence interval (CI), marked with black and white filled circles respectively.

663 Note that the colour scaling for the temporal TPL exponents is non-linear and

664 differs between the two maps.

665

666

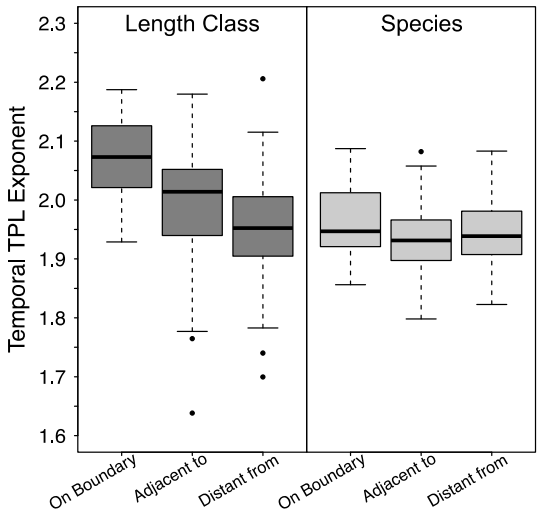

667

668 Figure 5:

669 Box plot showing the distribution of temporal of $\hat{\beta}(t,l)_s$ (left hand panel) and

670 $\hat{\beta}(t,p)_s$ (right hand panel) against hydrographic boundary assignment for 169

671 subareas.

672

673

674

675

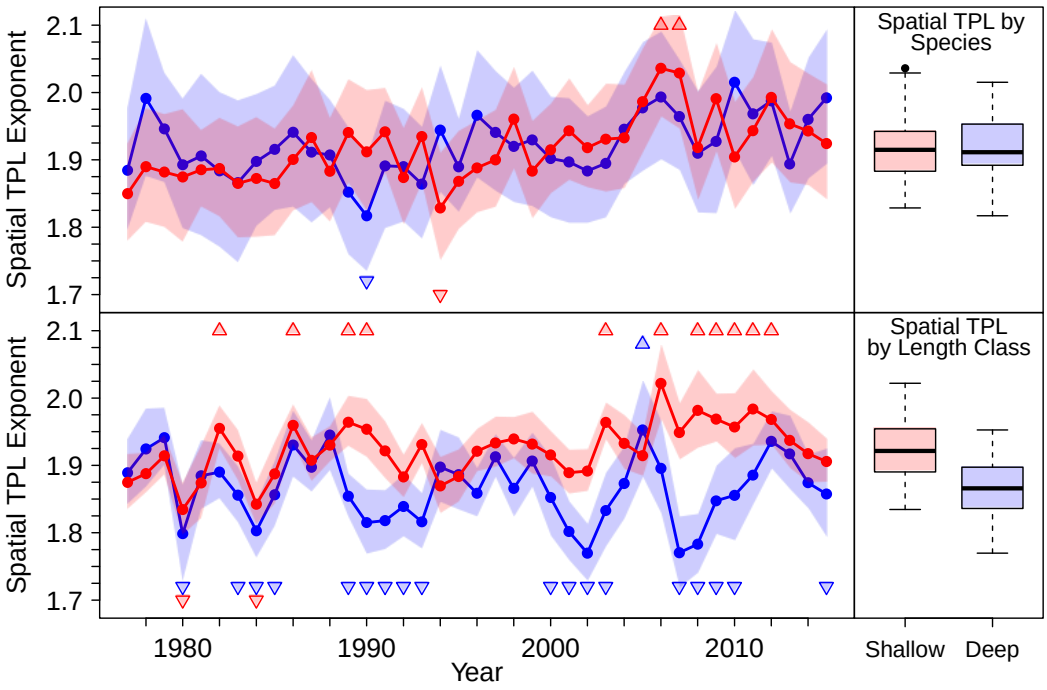

676

677 *Figure 6:*

678 Time-series of $\hat{\beta}(s_z, p)_t$ (top panels) and $\hat{\beta}(s_z, l)_t$ (bottom panels) calculated

679 separately for deep (>50m, blue, $z = d$) and shallow (≤50m, red, $z = sh$) regions of

680 the North Sea. Confidence intervals of 1.96 standard errors of the regression

681 estimates are plotted as opaque polygons to show periods of overlap and

682 divergence. Years with TPL exponents either above or below their 95%

683 confidence intervals are marked by triangles either above or below the time-

684 series respectively. The distributions of estimates over the whole period are

685 shown in adjacent box plots.

686

687

688

689

690

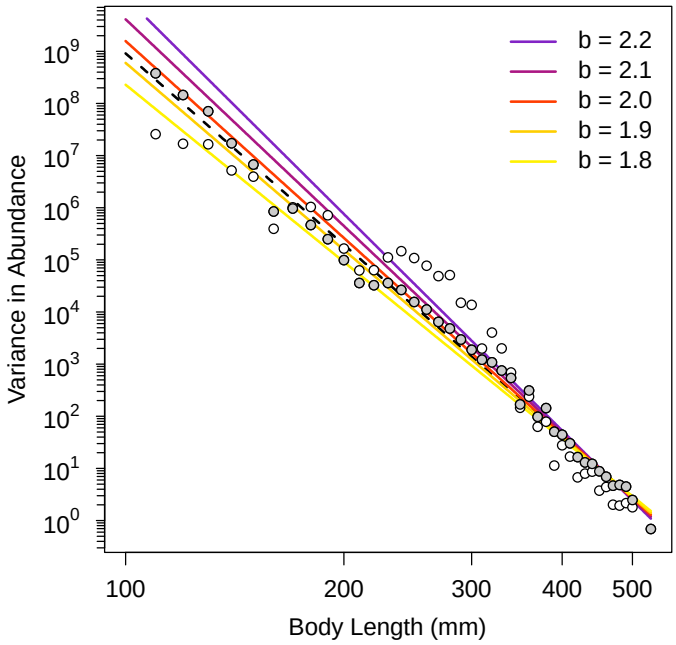

Figure 7:

The relationship between individual body size, variance in abundance, and a changing TPL exponent, using subarea "37F7" as an example (Figure 3). The estimated temporal TPL (black dashed line, $\beta = 1.94$) plotted as a function of body size where the mean abundance at body size is described by the empirically estimated size spectrum ($\log_{10}(\text{Mean Abundance}) = 16.7 - 6.27 \times \log_{10}(\text{Body Length})$, $p < 0.001$). Coloured lines illustrate the effect of changing $\beta(t)$, where the value of $\beta(t)$ is varied (holding all other terms constant) over the observed empirical range of $\beta(t)$ estimated across the North Sea (Figure 4). An increasing exponent results in a greater increase in variance at smaller body sizes. Raw body length – variance in abundance data are plotted as white circles. Note that the data show curvature, reflecting the curvature of the empirical size spectrum (coefficient of second order polynomial = -1.49, $p < 0.001$). However variance data that are adjusted by the squared difference between raw mean

abundance values and those estimated by the log-log linear size spectrum (grey circles) closely track the graph of the empirical estimate of TPL by body size. Note that the axes are on a logarithmic scale.

Table 1:

Summary statistics of each form of TPL exponents calculated. Number of p/l is the number of mean-variance pairs used to calculate log-log linear regressions. Number of t/s is the number of observations used to estimate mean-variance pairs. The mean range in abundance is the orders of magnitude over which log-log linear regressions are estimated.

Form of TPL	Number of β	Median Number of p/l per β	Median Number of t/s per p/l	Mean R-squared	Mean range in abundance
$\hat{\beta}(t,p)_s$	169	21	39	0.973	3.99
$\hat{\beta}(t,l)_s$	169	46	39	0.981	3.60
$\hat{\beta}(s_d,p)_t$	39	45	85	0.975	4.64
$\hat{\beta}(s_d,l)_t$	39	87	92	0.985	4.29
$\hat{\beta}(s_s,p)_t$	39	45	67	0.982	4.75
$\hat{\beta}(s_s,l)_t$	39	72	74	0.992	4.48